Article

Finite Element and Experimental Analysis of an Axisymmetric Electromechanical Converter with a Magnetostrictive Rod

Dorota Stachowiak * and **Andrzej Demenko**

Institute of Electrical Engineering and Electronics, Poznan University of Technology, Piotrowo 3A,
60-965 Poznan, Poland; andrzej.demenko@put.poznan.pl
* Correspondence: dorota.stachowiak@put.poznan.pl

check for
updates

Abstract: The paper presents the numerical and experimental investigations of the axisymmetric magnetostrictive actuator with a Terfenol-D rod. The applied model consists of equations that describe the magnetic and mechanical displacement fields. The equations of both fields are coupled through a nonlinear magneto-mechanical constitutive law. The model is considered as 2D axisymmetric. The finite element method is used to solve the field equations. Special attention is paid to the proper definition of magneto-mechanical relations. These relations are formed from measurements. A unique test stand is designed for the experimental investigation. The selected results of the simulation are compared with the measurement results. The comparison shows that the applied numerical model is sufficiently accurate.

Keywords: giant magnetostrictive materials; magneto-mechanical effects; magnetostrictive strain; Terfenol-D rod; giant magnetostrictive actuators; finite element analysis

1. Introduction

In recent years, thanks to the achievements of materials science, it is becoming possible to produce active components of an electromechanical converter from giant magnetostrictive materials (GMM). The GMM have a special property of exhibiting coupling between macroscopic mechanical (stress σ and strain ε) and magnetic variables (field intensity H and flux density B) [1–3]. This coupling is used to obtain a macroscopic extension known as magnetostriction. In general, the term magnetostriction refers to strains generated during the paramagnetic to ferromagnetic phase transition, i.e., spontaneous magnetostriction, or in response to an applied field, which constitutes magnetomechanical coupling. The magnetostriction occurs in the most ferromagnetic materials and leads to many effects [1–3]. The characteristic behavior of the magnetostrictive materials is caused by the reorientation of the magnetic dipoles within the material under the presence of the external magnetic field. This reorientation leads to shape change in sample dimensions, in the direction of the applied field, i.e., the Joule effect. The Joule effect corresponds to a longitudinal change in length due to the applied magnetic field. A positive Joule magnetostriction means elongation, whereas a negative magnetostriction indicates contraction. The Villari effect is the inverse of the Joule effect and corresponds to the change in magnetization due to the stress applied to the material. The Joule effect makes the GMM usable in actuation, while the Villari effect is useful for sensing. The GMM are widely employed nowadays as the main components of actuators [4–6], sensors [1,7,8], energy harvesters [9,10] or some other devices [1,3,11,12]. The GMM can also be used to build unconventional motors, so-called vibromotors [13,14].

The most popular kind of GMM is Terfenol-D, an alloy made of iron (Fe) and two rare earth elements: terbium (Tb) and dysprosium (Dy). Therefore, we concentrate on the system with a rod

made of Terfenol-D. The main area where Terfenol-D is applied is the construction of actuators and sensors. Giant magnetostrictive actuators (GMAs) are used in high-class industrial devices (linear motors, micropumps, microvalves, micropositioners, etc.,), biomedical applications and the arms industry [1,3].

The simplest form of the GMA consists of a cylindrical rod which is magnetically excited by the coil surrounding the rod to generate strain and force. Figure 1. shows a typical structure of the GMA that has been considered in this paper. The magnetostrictive rod (Terfenol-D) is coaxially installed in the center of the surrounding solenoid coil. The GMM rod needs pre-pressure produced by a pre-stress spring, because the magnetostrictive strain of the Terfenol-D rod can be enhanced by the axial compressive pre-stress σ_0 [1,15]. Thus, when a sufficient magnetic field is applied along the axis of the rod under the pre-stress, all the magnetic domains will rotate in the axial direction causing greater relative elongation, i.e., the magnetostrictive strain in the conventional sense [16]. In addition, the value of the maximum magnetostrictive strain increases with the increase of the compressive pre-stress [1,16].
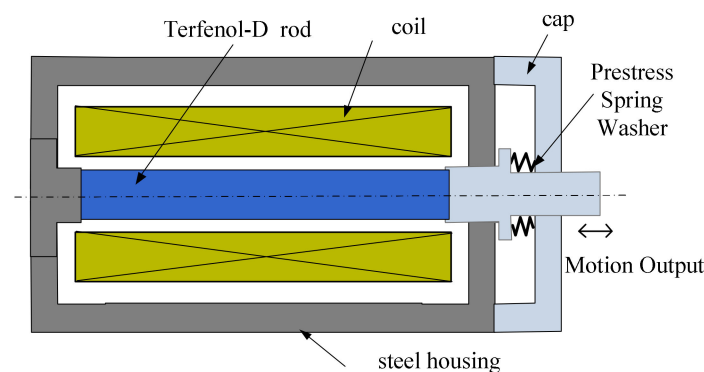

Figure 1. The structure diagram of the giant magnetostrictive actuators (GMA).

The GMA exhibits nonlinear behavior and magneto-mechanical coupling characteristics. In order to design the GMAs, accurate modeling of their characteristics is necessary. Usually, to determine the distribution of the magnetic and mechanical displacement fields, the finite element method (FEM) is used. Several studies about the use of FEM to solve nonlinear electro-magneto-mechanical equations and analyze the characteristics of the GMA have been published [12]. As examples, in [17,18], the authors implemented nonlinear FEM in static or quasi-static conditions. Fully coupled nonlinear magneto-elastic models for magnetostrictive transducers are presented in [19,20]. However, the resulting model equations presented in [19,20] are coded into the commercial finite element package COMSOL, which is used for meshing and global assembly of matrices.

The paper presents a finite element (FE) coupled model of the GMA. The proposed model consists of equations of the magnetic and displacement fields. The equations are coupled through a nonlinear magneto-mechanical constitutive law for a magnetostrictive rod. The model is considered to be 2D axisymmetric. In the developed model, we apply the concept of edge element calculations for a magnetic field and a special method of force calculations as well as using the modified Newton–Raphson algorithm to solve the nonlinear equations.

The paper is organized as follows: Section 2 describes the magneto-mechanical equations, while Section 3 presents the FE model of an axisymmetric electromechanical converter with a magnetostrictive rod. Section 4 shows validation of the FE model with an appropriate measurement setup. The article ends with conclusions.

2. Magnetomechanical Equations

The magnetomechanical effect consists of two coupled mechanisms: the applied stresses cause the magnetic moments to rotate, thus changing the magnetization, and the rotation of the moments to align

with the applied field generates strain in the material. In the magnetostrictive material, the strain ε and the magnetic flux density B are functions of the stress σ and the magnetic field intensity H. The behavior of the magnetostrictive materials is described by nonlinear relations, $\varepsilon = \varepsilon(\sigma,H)$, $B = B(\sigma,H)$ [1]. Here, the total strain tensor ε is the sum of the elastic strain ε_e and the magnetostrictive strain ε_{ms},

$$\varepsilon = \varepsilon_e + \varepsilon_{ms}. \tag{1}$$

Only the elastic strain contributes to mechanical stress [1,4]. The magnetostrictive strain describes the relative change in length of the material from the ordered but unaligned state to the state where domains are aligned.

Very often, the magnetostrictive strain is modeled using the linear constitutive relation, $\varepsilon_{ms} = dH$, where d is the piezo-magnetic strain matrix. However, in reality, the relation between the strain ε_{ms} and intensity H is nonlinear. The magnetostrictive strain exhibits a quadratic dependence on magnetization in a manner analogous to a quadratic polarization dependence exhibited by electrostrictive materials and piezoelectric compounds in high drive regimes [3,21]. This quadratic dependence is described by the magnetostrictive strain represented by the following deviatoric tensor:

$$\varepsilon_{ms} = \frac{3}{2}\frac{\lambda_s}{M_s}\mathrm{dev}\,M \otimes M, \tag{2}$$

where λ_s is the saturation magnetostriction constant, M_s is the saturation magnetization and M is the magnetization vector.

In the applied 2D axisymmetric model, the components of the strain tensor are defined as follows:

$$\varepsilon_{ms,u} = \frac{3}{2}\lambda_s\left(\frac{M_u}{M_s}\right)^2, \ (u = r, z), \tag{3}$$

where $\varepsilon_{ms,u}$ and M_u represent the u-th ($u = r, z$) component of the tensor ε_{ms} and the vector M respectively.

The vector of the magnetization M can be defined as

$$M = B(\nu_0 - \nu), \tag{4}$$

where ν_0 is the reluctivity of free space and ν is the reluctivity.

Saturation magnetostriction quantifies strains due to magneto-mechanical coupling and provides a metric for the characterization of the transduction capabilities of the material. The saturation magnetostriction attains different values under different pre-stress conditions. In the case of GMM, the saturation magnetostriction value under compression pre-stress is larger than the value under tension pre-stress; moreover, it increases with the increase of the compression pre-stress [1,3].

The saturation magnetization determines to what extent the magnetic moments can reorient in response to the applied field; therefore, to achieve strong transduction, its quantity should be large. Generally, the saturation magnetization is independent of the pre-stress [3].

According to Hook's law, the stress tensor σ is linked to the strain tensor ε_e by the elastic constitutive law:

$$\sigma = C\varepsilon_e = C\varepsilon - C\varepsilon_{ms}, \tag{5}$$

where C is the stiffness matrix [4,15] widely used in structural analysis.

Certain Terfenol-D compositions can be treated as isotropic materials [1]. In such cases, the constitutive law can be written using the Young's modulus of elasticity E and Poisson's ratio ν [4,22].

The stress tensor σ is linked to the strain tensor ε_e, while ε_e is expressed in terms of the elastic displacement vector u_e. The strain displacement relations can be written in the following form:

$$\varepsilon_e = Du_e = Du - Du_{ms}, \tag{6}$$

where D is the displacement gradient tensor [4,22] and u, u_{ms} represent the total displacement vector and the magnetostrictive displacement vector respectively.

Using the strain displacement relations (6), constitutive law (5) and creating a force balance condition under static equilibrium, we obtain the following governing equation:

$$- \mathrm{div}(CDu) = f + f_m + f_{ms}, \tag{7}$$

where f is the external force vector, $f_m = f_m(B)$ is the magnetic force vector and $f_{ms} = f_{ms}(\sigma, B)$ is the magnetostrictive force vector that depends on the stress σ and magnetic flux density B.

In the considered magnetomechanical problem, Equation (7) is coupled with the equations of the magnetic field and relations that express forces using magnetic field distribution. Here, the magnetic vector potential formulation is applied ($B = \mathrm{curl}A$). Thus, the equation describing the magnetic vector potential A for a given current density J is as follows:

$$\mathrm{curl}(\nu \mathrm{curl}A) = J + J_{ms}, \tag{8}$$

where $J_{ms} = J_{ms}(\sigma, B)$ is the magnetizing current induced by mechanical stress (Villari effect), representing the influence of magnetostriction on the magnetic field. In the calculations, the eddy currents are neglected, and J represents the density of a given current in the coil.

One could easily notice that (7) and (8) are coupled with each other through the sources.

3. Model of the GMA

The brittle nature of Terfenol-D and its poor machinability restricts its availability to geometries like cylindrical rods. The GMA contains components that are all cylindrical in nature with axisymmetric geometry that is well adapted to a built-in magnetostrictive transducer. The computations are performed in an axial symmetry domain with cylindrical coordinates (r, z, ϑ)—see Figure 2. The fundamental dimensions of the considered GMA are shown in Figure 2.
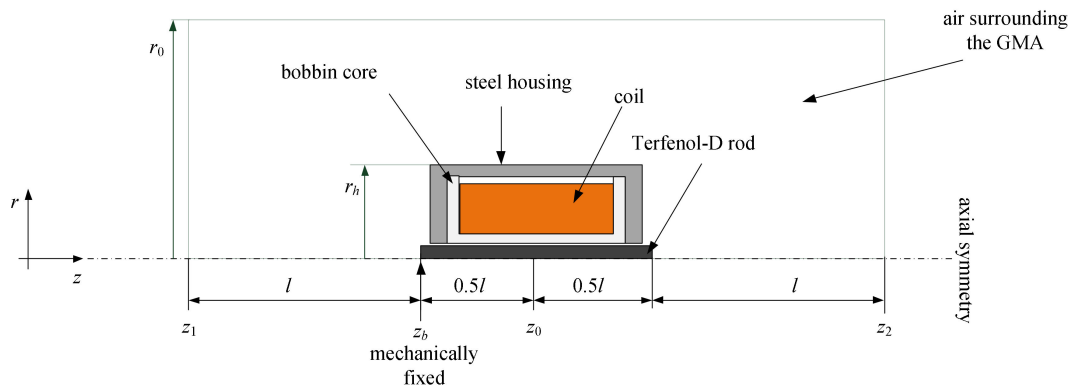

Figure 2. The geometry used for the finite element analysis of the GMA.

The actuator is surrounded by empty space and therefore it can be assumed that in the outer cylindrical surface $r = r_0 = 2.5r_h$ and plane surfaces $z = z_1 = z_0 - 1.5l$; $z = z_2 = z_0 + 1.5l$, the components of magnetic flux density are equal to zero. The boundaries for the region with the mechanical displacement field are placed off the contour surface of the magnetostrictive rod, i.e., the Terfenol-D rod. The boundary conditions for the Terfenol-D rod are of a symmetrical type and free (unconstrained) for the side situated on the symmetry axis. The Terfenol-D rod is one-sidedly, mechanically attached to the bottom $z = z_b$, see Figure 2. Thus, in the computations, the distortions of the steel housing and coil are neglected.

In the case of a clamped Terfenol-D rod, the total displacement remains zero, $u = 0$, since the magnetostrictive strain is compensated by elastic strain. Thus, in (5), $\varepsilon_e = -\varepsilon_{ms}$ and the second component of (5) represents the blocked stress σ_{block} of the material,

$$\sigma_{block} = -C\varepsilon_{ms}. \tag{9}$$

The blocked force refers to the maximum value of the magnetostrictive strain that can be applied to a sample of magnetostrictive materials. However, the blocked force can be calculated for each value of magnetic field intensity,

$$\mathbf{F}_{block} = -C\varepsilon_{ms} -_{\max} S_T, \tag{10}$$

where S_T is the vector of one nonzero component related only to the cross-sectional area of the GMM rod.

Magnetomechanical Equations (7), (8) are solved using the FE method, where the same mesh of elements is used for both magnetic and elastic computations. Therefore, the deformations determined on the mechanical grid accompanied by a change of dimensions are automatically transferred to a model describing the magnetic field.

In the FE method, Equations (7), (8) are represented by a matrix equation, which can be expressed in the following matrix form:

$$\mathbf{S}\varphi = \Theta + \Theta_{ms}(\sigma, \mathbf{B}), \tag{11}$$

$$\mathbf{K}\mathbf{U} = \mathbf{F} + \mathbf{F}_m(\mathbf{B}) + \mathbf{F}_{ms}(\sigma, \mathbf{B}), \tag{12}$$

where S and K are the magnetic and mechanical stiffness matrices, respectively, Θ is the current source vector, $\Theta_{ms}(\sigma, B)$ is the magnetostrictive current source vector, and φ is the vector of the edge value φ_i of the potential A.

For the oriented edge P_iP_j, the edge value is equal to the line integral of A on P_iP_j. The edge value of A for the edge P_iP_j can be considered as a loop flux in the loop around P_iP_j. The considered model is discretized using the element presented in Figure 3.

$\varphi_{2,5}$ is the edge value of A for edge P_2P_5 and corresponds to the loop flux in the loop around edge P_2P_5.
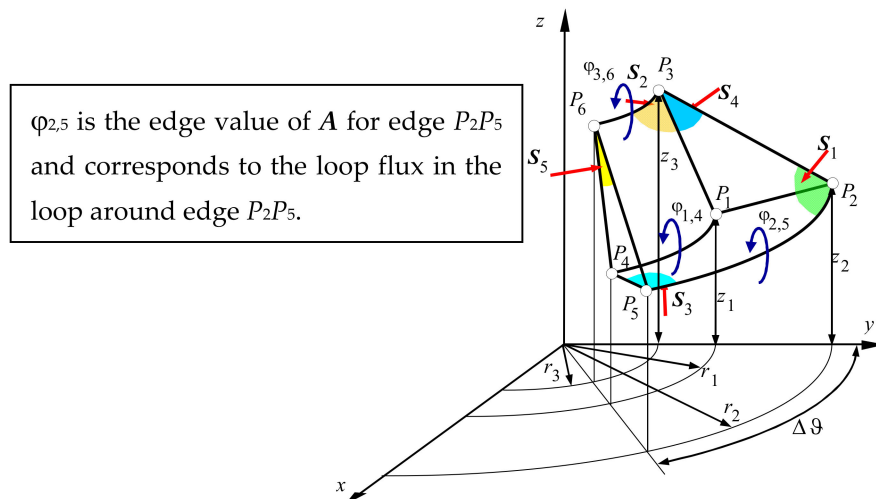
Figure 3. Finite element—curved, 5 faced-prism.

In the case of 3D, this element is a curved, 5-faced prism, but if we consider an axisymmetric model, then $\Delta\vartheta = 2\pi$, $y = r$ and $A = \mathbf{1}_\vartheta A_\vartheta$. For a node of coordinates $z = z_i$, $r = r_i$, $\varphi_i = 2\pi r_i A_\vartheta(z_i, r_i)$, where A_ϑ is the azimuthal component of the vector A. Taking advantage of the geometrical structure of the considered GMA, the calculations are performed in an axial-symmetric domain with cylindrical coordinates (r, z, ϑ).

The vector U in (12) represents nodal displacement in the direction of r and the z axis. F is the vector of external forces, $F_m(B)$ is the magnetic force vector, which is given by the local application of the virtual work principle and $F_{ms}(\sigma,B)$ is the vector of nodal magnetostrictive forces.

In the formulations of the above Equations (11), (12), we applied the idea presented in [17]. This idea was modified by applying the concept of edge element calculations for a magnetic field and by a special method of force calculations $F_m(B)$. The modifications of [17] consisted of considering the discretization grid as a grid composed of the elements shown in Figure 3. In the formulations of the magnetic force calculations, we applied the approach presented in [23]. The idea of the global force calculations presented in [23] was adopted for the calculations of force acting on each separately considered element.

The coupled problem was considered as an iterative process of subsequent magnetic and mechanical finite element calculations. This is a weak approach to coupling, as opposed to a strong coupling based on simultaneous iterations. The FE equations can be solved using a cascade procedure similar to the approach presented in [24].

The use of the personally developed software allows the introduction of the coupling by the use of the experimental data, which were obtained from a specially designed unique test stand for the experimental investigation characterization of Terfenol-D rods. Moreover, we calculated the $B(\sigma_0,H)$ characteristics according to the applied pre-stress σ_0 using our in-house developed software [15]. First, we assumed the initial stress σ_0 and then we solved nonlinear magnetostatic equations (see Figure 4).
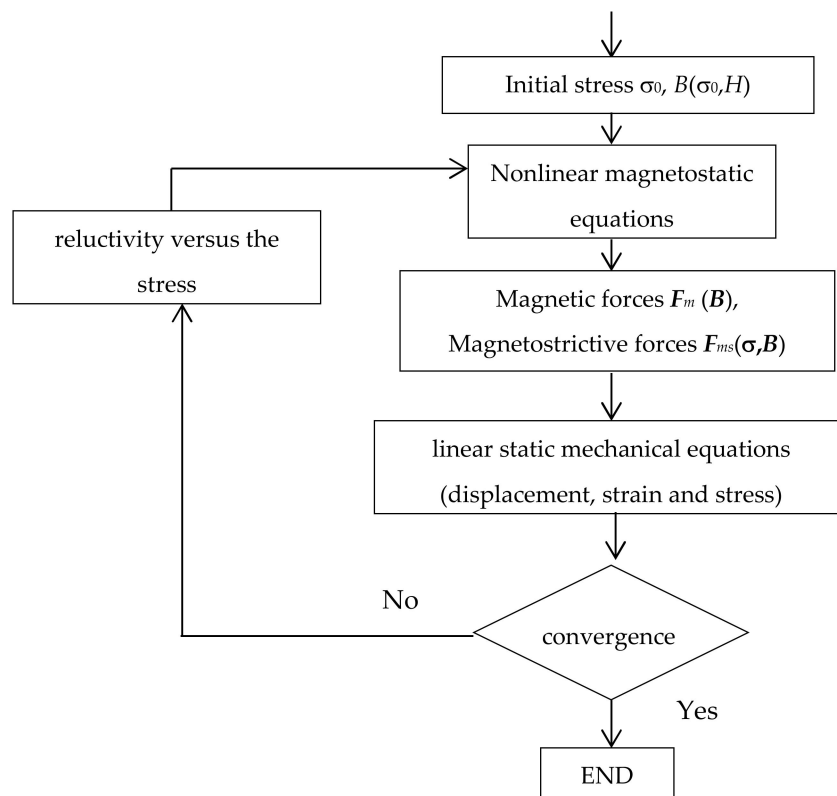
Figure 4. Diagram of the weak coupling model.

The modified Newton–Raphson algorithm was applied to solve the nonlinear equations. We used some ideas presented in paper [25]. In the applied method, the classical Jacobian matrix is replaced by its simplified representations S_{sJ}. In order to obtain S_{sJ}, the reluctivity ν in the description entries of formulas of the matrix is replaced by dH/dB, i.e., by $d(|B|\nu)/d(|B|)$. The increments, i.e., $S_{sJ}^{-1}r^{(k)}$, are calculated using the Cholesky decomposition procedure. Thus, the matrix S_{sJ} is expressed by the product of triangular matrices, i.e., $S_{sJ} = LL^T$. In the applied algorithm, the matrices S_{sJ} and L are

calculated only for the first five iteration steps and for the $(k+1)$-th step, if $|r^{(k)}|/|r^{(k-1)}| > 0.99$ where r is the residual vector.

In the next step, the magnetic forces $F_m\,(B)$ are calculated using the local application of the virtual work principle and the magnetostrictive forces $F_{ms}(\sigma,B)$ are calculated using a similar approach to the one presented in [24]. Then, mechanical equations are solved.

The calculations were performed for a grid with different numbers of elements. The considered GMA was divided into the elements shown in Figure 3 but was adapted to the axisymmetric model. The results for a model of 120,000 elements are presented in the next section.

4. Computed and Experimental Results

The FE model presented above was applied for the analysis of the converter specially prepared for experimental testing (Figure 5b). The magnetostrictive rod of the converter was made of Terfenol-D. The length of the rod was 100 mm and the diameter was 10 mm (Figure 5a). When designing the test stand, various techniques to measure small displacements of the rod were taken into account. To obtain convergent displacement measurements, we used, among others, a micrometer sensor (Figure 5c). A laser sensor was also applied.
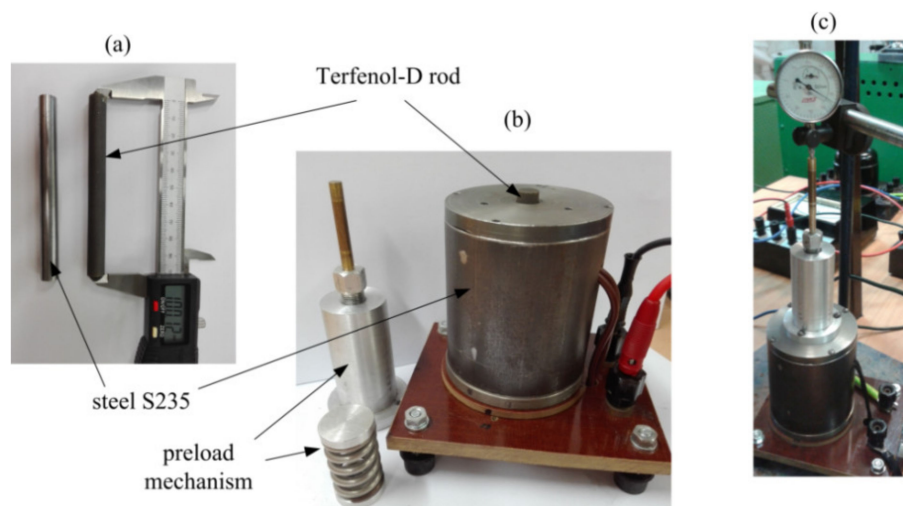

Figure 5. A sample of Terfenol-D and steel S235 (**a**), The prototype of the GMA for laboratory measurements (**b**), experimental setup (**c**).

The results of the FE method were used in the calculations of the selected field and integral quantities, e.g., stresses, strains, magnetic field density, displacements and blocked force. It was assumed that a GMA was supplied by a DC power source. It should be noted that the calculations were preceded by the measurement of nonlinear characteristics of the magnetic materials of the tested converter. The magnetic measurement was performed in an open magnetic circuit [26]. Demagnetizing factors for a cylindrical Terfenol D rod were defined using the ballistic method [26]. The measured magnetization characteristic is presented in Figure 6.
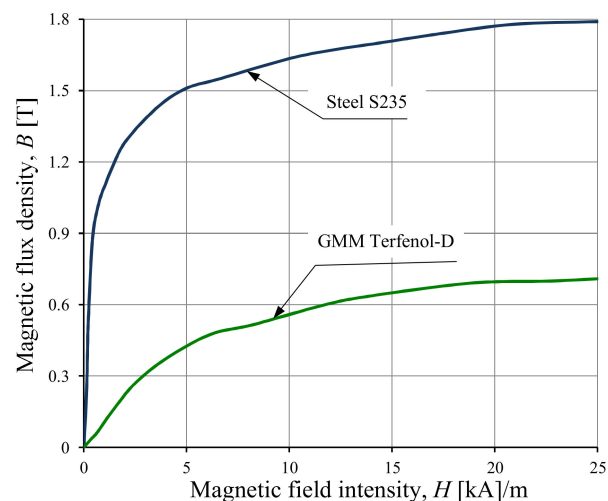
Figure 6. Measured magnetization characteristic of the materials used in the finite element (FE) model.

The performance of a magnetostrictive converter strongly depends on the initial values of magnetic field intensity and stresses. Thus, these values should be selected appropriately. Studying coupled magnetomechanical properties of a magnetostrictive converter ought to be very thorough and should take place during its operation, since the expected operating range is obtained by applying mechanical pre-stress. The authors previously computed the $B(\sigma_0, H)$ characteristics according to the applied pre-stress σ_0, using their own in-house developed software [15]. The calculations were performed for the properties of Terfenol-D, a description of which was found in the literature [15]. Here, in order to fully recognize the properties, additional tests were completed, e.g., the tested rod was subjected to strong stress. Monolithic Terfenol-D is very brittle and can easily be damaged. The damaged sample of the Terfenol-D rod is presented in Figure 7. A laser scanning confocal microscope (LSM) (LSM 710 Zeiss) was used to characterize the Terfenol-D surface [27].
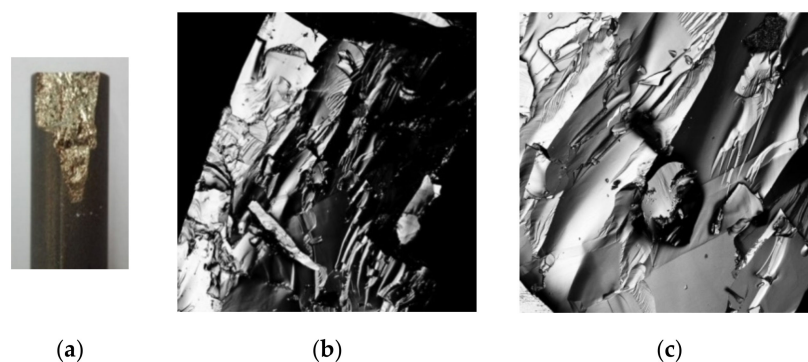

| (**a**) | (**b**) | (**c**) |

Figure 7. The damaged sample of Terfenol D rod (**a**) Microscope image of surface of Terfenol D (**b**) EC Epiplan-Neofluar 20x/0.50 HD DIC M2424.89 μm, y: 424.89 μm (**c**) EC Epiplan-Neofluar 50x/0.80 HD DIC M27 x: 169.96 μm, y: 169.96 μm.

The calculated magnetic field line and magnetic flux density distribution for the GMA at a pre-stress of 7.2 MPa and a supply current of 6 A have been shown in Figure 8a,b. It is well known that for the correct operation of a magnetostrictive converter, the most important factors are distributions of strain and a displacement field in a Terfenol-D rod. These distributions have been shown in Figure 8c,d. It has been assumed that the rod is mechanically fixed, however, it can move freely.
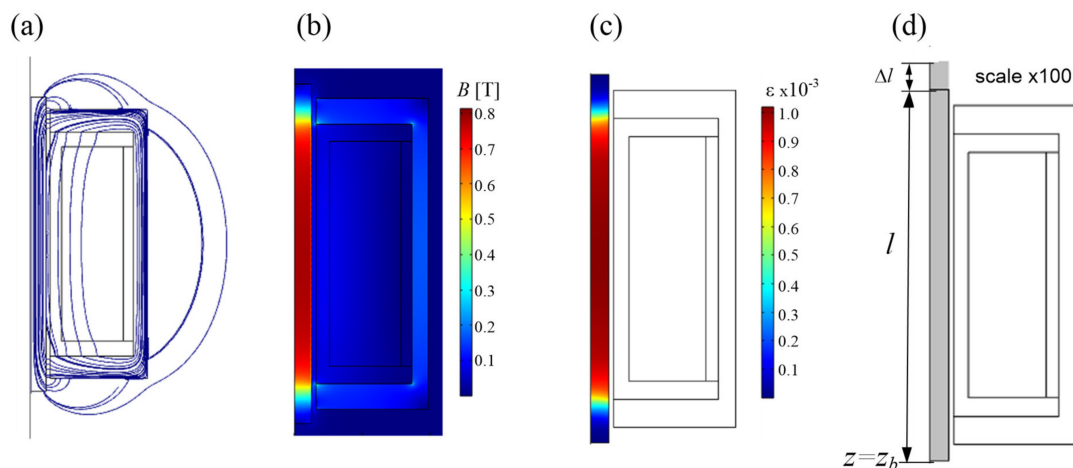
Figure 8. Distribution of the magnetic field line in the GMA (I = 6 A, σ_0 = 7.2 MPa) (**a**); distribution of the magnetic flux density in the GMA (**b**); distribution of the strain in the Terfenol-D rod (**c**); the scaled deformations of displacement of the Terfenol-D rod (**d**).

The presented distributions of magnetic field shows that the magnetic field is concentrated at the center of the rod. The intensity and uniformity of the magnetic field are the key factors that influence the performance of a GMA. The magnetic field changes direction at the ends of the rod. On the basis of the presented results, it can be seen that the total strain is concentrated at the center of the rod due to the high concentration of the magnetic field in the middle of the rod.

In Figure 9, the selected results of calculations and measurements are given. The calculated and measured values of the output displacement of the GMA as a function of supplied current are shown (see Figure 9).
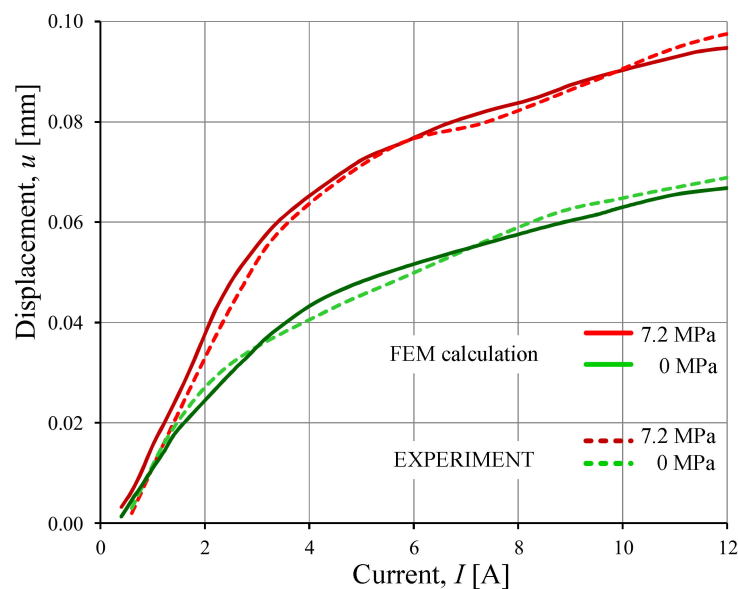

Figure 9. The displacement of the GMA vs. the supply current.

When we modeled the magnetostrictive strain by using the linear constitutive relation ($\varepsilon_{ms} = d\,H$), we obtained results with large errors. For example, the measured value of displacement for the supply current I = 3 A and pre-stress σ_0 = 7.2 MPa was u = 0.052 mm. The result of the displacement calculation for the linear model was u = 0.060 mm, while for the nonlinear model, it was u = 0.055 mm (see Figure 9). The difference between the calculated value of the displacement for the linear model

and the measured value of the displacement exceeded 15%, while the difference between the non-linear model and the measured value was smaller than 6%.

The calculated blocked force of the GMA as a function of supply current is shown in Figure 10. To determine the blocked force, it was assumed that the Terfenol-D rod was clamped.
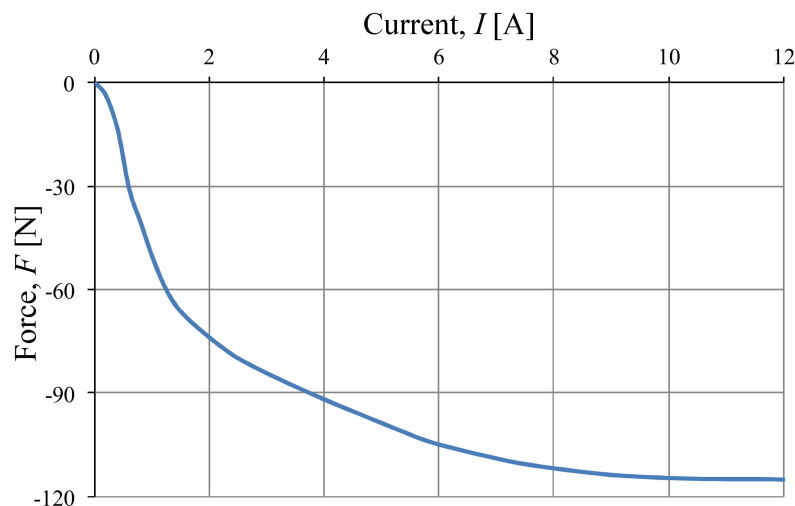
Figure 10. The blocked force of the GMA vs. the supply current.

The above results show that the proposed numerical model of a giant magnetostrictive actuator can be a useful tool for optimizing the device geometry and material selection.

5. Conclusions

The finite element model for a giant magnetostrictive actuator has been presented. The elaborated model allows one to take magnetomechanical coupling as well as material's nonlinearity into account. The measured nonlinear characteristics of the magnetic materials of the tested converter were applied in the finite element model. The elaborated model can predict behavior of the magnetostrictive materials and can be used as a tool for the design process of the magnetostrictive converter.

A special test stand was designed for an experimental investigation. The predictions related to the use of the numerical method were verified with selected experimental measurements. The investigations showed that carrying out the field analysis of the magnetostrictive transducer requires accurate knowledge of the properties of the used magnetostrictive materials.

The developed software enables the analysis of coupled magnetomechanical phenomena and allows for the determination of the characteristics that are hard to measure. The blocked force is an example of such a difficult to measure quantity.

The presented results relate to the prototype that was created for the experimental verification of the elaborated magnetomechanical model of axisymmetric electromechanical converter with a magnetostrictive rod. Further research will formulate guidelines for optimal design of an axisymmetric magnetostrictive converter. The existing model will be extended for the modeling of thermal effects. The elaborated model will be coupled with the optimization procedure.

References

1. Engdahl, G. *Handbook of Giant Magnetostrictive Materials*; Academic Press: San Diego, CA, USA, 2000. [CrossRef]
2. Cullity, B.D.; Graham, C.D. *Introduction to Magnetic Materials*; Wiley-IEEE Press: Hoboken, NJ, USA, 2008; pp. 241–271. [CrossRef]
3. Smith, R.C. *Smart Material Systems: Model Development*; SIAM: Philadelphia, PA, USA, 2005. [CrossRef]
4. Stachowiak, D. Finite element analysis of the active element displacement in a giant magnetostrictive transducer. *COMPEL Int. J. Comput. Math. Electr. Electron. Eng.* **2016**, *35*, 1371–1381. [CrossRef]
5. Xue, G.; Zhang, P.; Li, X.; He, Z.; Wang, H.; Li, Y.; Ce, R.; Zeng, W.; Li, B. A review of giant magnetostrictive injector (GMI). *Sens. Actuators A Phys.* **2018**. [CrossRef]
6. Kowalski, K.; Nowak, L.; Knypiński, Ł.; Idziak, P. Influence of the core saturation on the dynamic performance of the magnetostrictive actuator. *Arch. Electr. Eng.* **2017**, *66*, 523–531. [CrossRef]
7. Sauer, S.; Marschner, U.; Adolphi, B.; Clasbrummel, B.; Fischer, W.-J. Passive wireless resonant Galfenol sensor for osteosynthesis plate bending measurement. *IEEE Sens. J.* **2012**, *12*, 1226–1233. [CrossRef]
8. Pernía, A.M.; Mayor, H.A.; Prieto, M.J.; Villegas, P.J.; Nuño, F.; Martín-Ramos, J.A. Magnetostrictive Sensor for Blockage Detection in Pipes Subjected to High Temperatures. *Sensors* **2019**, *19*, 2382. [CrossRef]
9. Deng, Z.; Dapino, M.J. Review of magnetostrictive vibration energy harvesters. *Smart Mater. Struct.* **2017**, *26*, 103001. [CrossRef]
10. Ahmed, U.; Jeronen, J.; Zucca, M.; Palumbo, S.; Rasilo, P. Finite element analysis of magnetostrictive energy harvesting concept device utilizing thermodynamic magneto-mechanical model. *J. Magn. Magn. Mater.* **2019**, *486*, 1–8. [CrossRef]
11. Andrés-Mayor, H.; Prieto, M.J.; Villegas, P.J.; Nuño, F.; Martín-Ramos, J.A.; Pernía, A.M. Development of Magnetostrictive Transducer Prototype for Blockage Detection on Molten Salt Pipes. *Energies* **2018**, *11*, 587. [CrossRef]
12. Apicella, V.; Clemente, C.S.; Davino, D.; Leone, D.; Visone, C. Review of Modeling and Control of Magnetostrictive Actuators. *Actuators* **2019**, *8*, 45. [CrossRef]
13. Cernomazu, D.; Raţă, M.; Ungureanu, C.; Niţan, I.; Prodan, C.; Olariu, E.; Milici, M.R.; Milici, L.D.; Romaniuc, I. Magnetostrictive Micro Motor with Reversible Rotation. Patent No. RO129322A2, 28 March 2014. Available online: https://worldwide.espacenet.com/patent/search/family/050343543/publication/RO129322A2?q=vibromotor (accessed on 28 February 2020).
14. Romaniuc, I. Magnetostrictive Vibromotors Using Terfenol-D Alloy, Buletinul Institutului Politehnic din Iaşi Automatic Control and Computer Science Section. 2013. Tome LIX (LXIII) Fasc. 1. pp. 31–39. Available online: http://www.usv.ro/q-doc/database/2010/10/publicate/04.pdf (accessed on 28 February 2020).
15. Stachowiak, D. The influence of magnetic bias and prestress on magnetostriction characteristics of a giant magnetostrictive actuator. *Przegląd Elektrotechniczny* **2013**, *89*, 233–236. Available online: http://www.pe.org.pl/articles/2013/4/53.pdf (accessed on 12 February 2020).
16. Zheng, X.J.; Liu, X.E. A nonlinear constitutive model for Terfenol-D rods. *J. Appl. Phys.* **2015**, *97*, 053901. [CrossRef]
17. Besbes, M.; Ren, Z.; Razek, A. A generalized finite element model of magnetostriction phenomena. *IEEE Trans. Magn.* **2001**, *37*, 3324–3328. [CrossRef]
18. Yan, R.; Wang, B.; Yang, Q.; Liu, F.; Cao, S.; Huang, W. A numerical model of displacement for giant magnetostrictive actuator. *IEEE Trans. Appl. Supercond.* **2004**, *14*, 1914–1917. [CrossRef]
19. Chakrabarti, S.; Dapino, M.J. Coupled axisymmetric finite element model of a hydraulically amplified magnetostrictive actuator for active powertrain mounts. *Finite Elem. Anal. Des.* **2012**, *60*, 25–34. [CrossRef]
20. Graham, F.C.; Mudivarthi, C.; Datta, S.; Flatau, A.B. Modeling of a Galfenol transducer using the bidirectionally coupled magnetoelastic model. *Smart Mater. Struct.* **2009**, *18*. [CrossRef]
21. Dapino, M.; Smith, R.; Flatau, A. Structural magnetic strain model for magnetostrictive transducers. *IEEE Trans. Magn.* **2000**, *36*, 545–556. [CrossRef]
22. Dym, C.L.; Shames, I.H. *Solid Mechanics*; Springer: New York, NY, USA, 2013. [CrossRef]
23. Demenko, A.; Łyskawiński, W.; Wojciechowski, R.M. Equivalent Formulas for Global Magnetic Force Calculation from Finite Element Solution. *IEEE Trans. Magn.* **2012**, *48*, 195–198. [CrossRef]

24. Delaere, K.; Heylen, W.; Hameyer, K.; Belmans, R. Local magnetostriction forces for finite element analysis. *IEEE Trans. Magn.* **2000**, *36*, 3115–3118. [CrossRef]

25. Demenko, A.; Nowak, L.; Pietrowski, W.; Stachowiak, D. 3D edge element analysis of saturation effects in a permanent magnet machine. *COMPEL Int. J. Comput. Math. Electr. Electron. Eng.* **2002**, *21*. [CrossRef]

26. Stachowiak, D.; Idziak, P. Investigation of magnetic properties of magnetostrictive materials and constructional steel. *Pozn. Univ. Technol. Acad. J. Electr. Eng.* **2016**, *85*, 95–106. Available online: http://yadda. icm.edu.pl/baztech/element/bwmeta1.element.baztech-de868144-6407-478f-9acf-89d2289bd881 (accessed on 12 February 2020). (In Polish).

27. Adamski, A.; Biadasz, A.; Domieracki, K.; Kojdecki, M.A.; Paukszta, D.; Uryzaj, D.; Wolarz, E. Morphology and molecular organisation of liquid-crystalline perylene-3,4,9,10-tetra-(n-hexylester) deposited on solid substrate. *Liq. Cryst.* **2015**, *42*, 456–462. [CrossRef]